

# Supplement to ‘Investigation of a Saharan dust plume in Western Europe by remote sensing and transport modelling’

Hengheng Zhang<sup>1</sup>, Frank Wagner<sup>1,2</sup>, Harald Saathoff<sup>1</sup>, Heike Vogel<sup>1</sup>, Gholam Ali Hoshyanipour<sup>1</sup>,  
5 Vanessa Bachmann<sup>2</sup>, Jochen Förstner<sup>2</sup>, Thomas Leisner<sup>1</sup>

<sup>1</sup>Institute of Meteorology and Climate Research, Karlsruhe Institute of Technology, Eggenstein-Leopoldshafen, 76344, Germany

<sup>2</sup>Deutscher Wetterdienst (DWD), Frankfurter Str. 135, 63067 Offenbach am Main, Germany

*Correspondence to:* Hengheng Zhang (hengheng.zhang@kit.edu)

## 10 S.1 Lidar ratio retrieval from scanning elastic lidar measurements

The aerosol lidar ratio is essential for retrieving optical parameters from elastic lidar when using the Klett-Fernald method and the value of it changes largely for aerosol with different chemical and physical properties(Groß et al., 2013). However, lidar ratio retrieval is not an easy task. To solve this problem, Raman lidar (Wandinger, 2005) and High Spectral Resolution lidar (HSRL) (Liu et al., 1999) can be used. However, the weak scattering cross-section of Raman scattering and the complex  
15 configuration of HSRL impeded the wide application of these two technologies. Therefore, it is still important to develop a robust and manoeuvrable method for retrieving the lidar ratio. Here we explain how we retrieved the aerosol lidar ratio using elastic lidar measurement at different observation angles.

This method was tested by simulated and experimental cases and verified mathematically. Firstly, we used a simulation to test this method. We constructed lidar signals based on the lidar equation at two elevation angles with the same aerosol backscatter  
20 coefficient profile. Then we retrieved backscatter coefficients at these two angles with different values of the lidar ratio using the Klett-Fernald method. The input (dash line) and retrieved (red and green line) backscatter coefficient profiles for different values of lidar ratio are shown in Fig. S1.1. The input lidar ratio used in the lidar equation for this simulation is 55 sr. Fig. S1.1. shows differences between input and retrieved profiles for lidar ratios not equal to the input lidar ratio (55 sr). More importantly, we found difference between the two retrieved profiles when the lidar ratios are not equal to the input lidar ratio  
25 (55 sr)

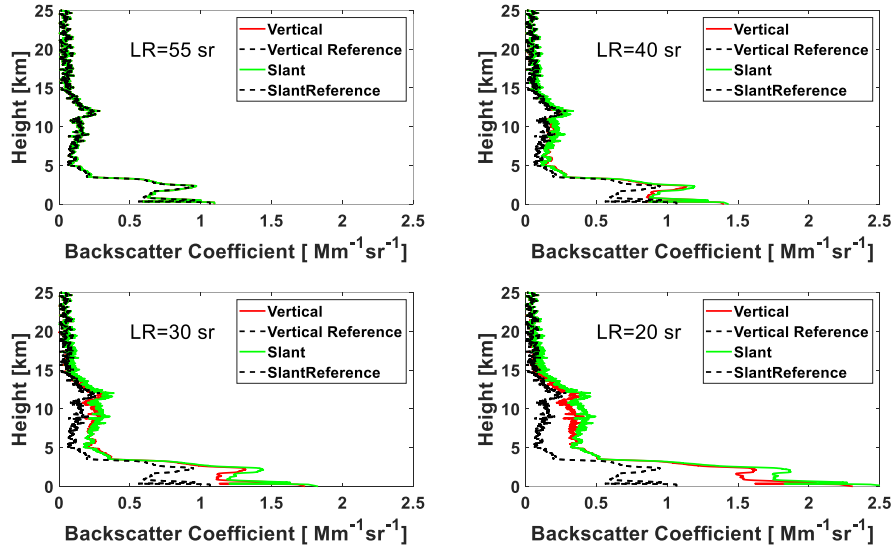


**Figure S1.1.** The input (dash line) and retrieved (red and green line) backscatter coefficient profiles for different values of the lidar ratio with an input lidar ratio of 55 sr.

30 To test the sensitivity of this difference with lidar ratio, we performed more simulations for different values of the lidar ratio. Fig. S1.2 shows the ratio between vertical and slant backscatter coefficients for different lidar ratios with input lidar ratios being 55 sr and 30 sr respectively. From this figure, we can identify the ratio equal to unity when the lidar ratio is equal to the input lidar ratio. Besides, a smaller value of a chosen lidar ratio caused the backscatter coefficient from the vertical retrieval being smaller than that from the slant retrieval, and vice versa.

35

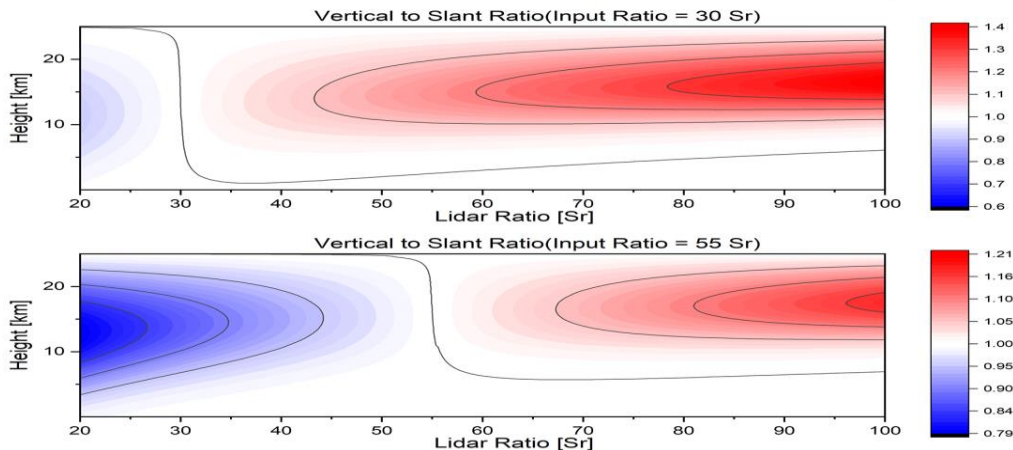


**Figure S1.2.** The ratio between vertical and slant backscatter coefficient for different values of the lidar ratio with input lidar ratio being 55 sr and 30 sr respectively.

Now we can use an observation to test this method, Fig. S1.3 shows vertical and slant backscatter coefficients from lidar measurements for different values of the lidar ratio from 20 sr to 50 sr. This case is from the Saharan dust event occurred from 19:21 to 22:47 (UTC) on 8<sup>th</sup>, April, 2018 and this dust layer existed at an altitude between 2.5~6 km. From this figure, we can see that an assumed lidar ratio at 50 sr showed consistent backscatter values between vertical and slant profiles in the dust layer. This is consistent with other observations showing that this value is a typical lidar ratio value for Saharan dust over Europe (Groß et al., 2013).

45

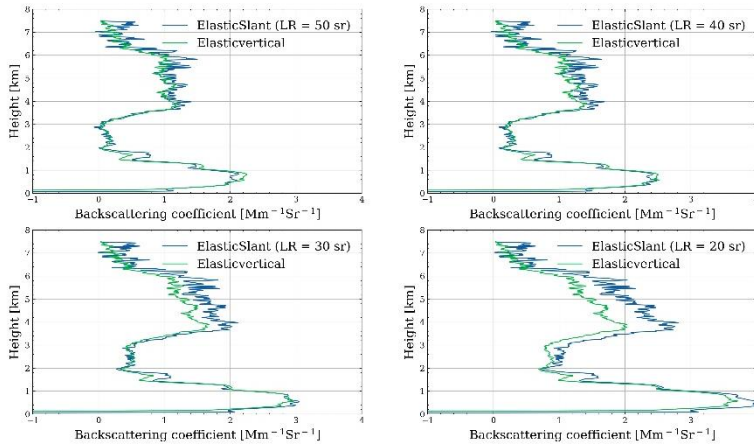


**Figure S1.3.** Vertical and slant backscatter coefficients from lidar measurements from 19:21 to 22:47 (UTC) on 8<sup>th</sup>, April, 2018 for lidar ratios ranging from 20 to 55 sr.

In conclusion, this method allows for retrieving the lidar ratio if assuming a horizontal homogenous atmosphere based on elastic lidar measurements at two different observation angles. A mathematical derivation is shown below:

$$P(r) = C_0 T_0^2 \frac{\beta_{aer}(r) + \beta_{mol}(r)}{r^2} \exp\left(-2 \int_0^r [\alpha_{aer}(r) + \alpha_{mol}(r)] dr\right) \quad (1)$$

$$\beta(r) = \frac{RCS(r) * \exp\left\{2 * (S_a - S_m) * \int_r^{R_{ref}} \beta_{mol}(r') dr'\right\}}{\frac{RCS(r)}{C * \beta_{mol}(r_{ref})} + 2 * S_a * \int_r^{R_{ref}} [RCS(r') * \exp\left\{2 * (S_a - S_m) * \int_r^{R_{ref}} \beta_{mol}(r'') dr''\right\}] dr'} \quad (2)$$

In term of the numerator,  $S_a$  is for the retrieval method and  $S_{a0}$  is for the input lidar ratio. Let elevation angle be  $\theta_1$  and  $\theta_2$ , and  $\theta_1 > \theta_2$ ,  $\mu_1 = \frac{1}{\sin \theta_1}$ ,  $\mu_2 = \frac{1}{\sin \theta_2}$ ,  $\mu = \mu_2 - \mu_1$ . For  $\theta_1$  direction:

55

$$P(\mu_1 r) = C_0 T_0^2 \frac{\beta_{aer}(\mu_1 r) + \beta_{mol}(\mu_1 r)}{(\mu_1 r)^2} \exp\left(-2 \int_0^{\mu_1 r} [\alpha_{aer}(\mu_1 r) + \alpha_{mol}(\mu_1 r)] dr\right) \quad (3)$$

$$\beta(\mu_1 r) = \frac{\text{RCS}(\mu_1 r) * \exp \left\{ 2 * (S_a - S_m) * \int_{\mu_1 r}^{\mu_1 r_{ref}} \beta_{mol}(\mu_1 r') dr' \right\}}{\frac{\text{RCS}(\mu_1 r)}{C * \beta_{mol}(\mu_1 r_{ref})} + 2 * S_a * \int_{\mu_1 r}^{\mu_1 r_{ref}} [\text{RCS}(\mu_1 r') * \exp \left\{ 2 * (S_a - S_m) * \int_{\mu_1 r'}^{\mu_1 r_{ref}'} \beta_{mol}(\mu_1 r'') dr'' \right\}] dr'} \quad (4)$$

For  $\theta_2$  direction:

$$P(\mu_2 r) = C_0 T_0^2 \frac{\beta_{aer}(\mu_2 r) + \beta_{mol}(\mu_2 r)}{(\mu_2 r)^2} \exp \left( -2 \int_0^{\mu_2 r} [\alpha_{aer}(\mu_2 r) + \alpha_{mol}(\mu_2 r)] dr \right) \quad (5)$$

$$60 \quad \beta(\mu_2 r) = \frac{\text{RCS}(\mu_2 r) * \exp \left\{ 2 * (S_a - S_m) * \int_{\mu_2 r}^{\mu_2 r_{ref}} \beta_{mol}(\mu_2 r') dr' \right\}}{\frac{\text{RCS}(\mu_2 r)}{C * \beta_{mol}(\mu_2 r_{ref})} + 2 * S_a * \int_{\mu_2 r}^{\mu_2 r_{ref}} [\text{RCS}(\mu_2 r') * \exp \left\{ 2 * (S_a - S_m) * \int_{\mu_2 r'}^{\mu_2 r_{ref}'} \beta_{mol}(\mu_2 r'') dr'' \right\}] dr'} \quad (6)$$

Replace the RCS in Equation (4) and Equation (6) by Equation (3) and Equation (5), respectively. Please note that  $\text{RCS} = P(r) * r^2$ . Equation (4) divided by Equation (6). . For numerator:

$$\begin{aligned} & \frac{\text{RCS}(\mu_1 r)_1 * \exp \left\{ 2 * (S_a - S_m) * \int_{\mu_1 r}^{\mu_1 r_{ref}} \beta_{mol}(\mu_1 r')_1 dr' \right\}}{\text{RCS}(\mu_2 r)_2 * \exp \left\{ 2 * (S_a - S_m) * \int_{\mu_2 r}^{\mu_2 r_{ref}} \beta_{mol}(\mu_2 r')_2 dr' \right\}} \\ &= \frac{k * [\beta_{aer}(\mu_1 r)_1 + \beta_{mol}(\mu_1 r)_1] * \exp \left\{ -2 \int_0^{\mu_1 r} [\alpha_{aer}(\mu_1 r') + \alpha_{mol}(\mu_1 r')_1] dr' \right\} * \exp \left\{ 2 * (S_a - S_m) * \int_{\mu_1 r}^{\mu_1 r_{ref}} \beta_{mol}(\mu_1 r')_1 dr' \right\}}{k * [\beta_{aer}(\mu_2 r)_2 + \beta_{mol}(\mu_2 r)_2] * \exp \left\{ -2 \int_0^{\mu_2 r} [\alpha_{aer}(\mu_2 r') + \alpha_{mol}(\mu_2 r')_2] dr' \right\} * \exp \left\{ 2 * (S_a - S_m) * \int_{\mu_2 r}^{\mu_2 r_{ref}} \beta_{mol}(\mu_2 r')_2 dr' \right\}} \\ 65 &= \frac{\exp \left\{ -2 \int_0^{\mu_1 r} [\alpha_{aer}(\mu_1 r') + \alpha_{mol}(\mu_1 r')_1] dr' \right\} * \exp \left\{ 2 * (S_a - S_m) * \int_{\mu_1 r}^{\mu_1 r_{ref}} \beta_{mol}(\mu_1 r')_1 dr' \right\}}{\exp \left\{ -2 \int_0^{\mu_2 r} [\alpha_{aer}(\mu_2 r') + \alpha_{mol}(\mu_2 r')_2] dr' \right\} * \exp \left\{ 2 * (S_a - S_m) * \int_{\mu_2 r}^{\mu_2 r_{ref}} \beta_{mol}(\mu_2 r')_2 dr' \right\}} \\ &= \frac{\exp \left\{ -2 \int_0^{\mu_1 r_{ref}} \alpha_{mol}(\mu_1 r')_1 dr' - 2 \int_0^{\mu_1 r} \alpha_{aer}(\mu_1 r')_1 dr' + 2 * S_a * \int_{\mu_1 r}^{\mu_1 r_{ref}} \beta_{mol}(\mu_1 r')_1 dr' \right\}}{\exp \left\{ -2 \int_0^{\mu_2 r_{ref}} \alpha_{mol}(\mu_2 r')_2 dr' - 2 \int_0^{\mu_2 r} \alpha_{aer}(\mu_2 r')_2 dr' + 2 * S_a * \int_{\mu_2 r}^{\mu_2 r_{ref}} \beta_{mol}(\mu_2 r')_2 dr' \right\}} \\ &= \frac{1}{\exp \left\{ -2 \int_0^{\mu r_{ref}} \alpha_{mol}(r') dr' - 2 \int_0^{\mu r} \alpha_{aer}(r') dr' + 2 * S_a * \int_0^{\mu r_{ref}} \beta_{mol}(r') dr' \right\}} \\ &= \frac{1}{\exp \left\{ -2 \int_0^{\mu r_{ref}} [\alpha_{mol}(r') - S_a * \beta_{mol}(r')] dr' - 2 \int_0^{\mu r} [\alpha_{aer}(r') + S_a * \beta_{mol}(r')] dr' \right\}} \\ 70 &= \frac{1}{\exp \left\{ -2 \int_0^{\mu r_{ref}} [S_m * \beta_{mol}(r') - S_a * \beta_{mol}(r')] dr' \right\} \exp \left\{ -2 \int_0^{\mu r} [S_{ain} * \beta_{aer}(r') + S_a * \beta_{mol}(r')] dr' \right\}} \end{aligned} \quad (7)$$

And for the denominator:

$$\begin{aligned}
& \frac{\frac{RCS(\mu_1 r_{ref})}{C * \beta_{mol}(\mu_1 r_{ref})}_1 + 2 * S_a * \int_{\mu_1 r}^{\mu_1 r_{ref}} RCS(\mu_1 r')_1 * \exp \left\{ 2 * (S_a - S_m) * \int_{\mu_1 r}^{\mu_1 r_{ref}} \beta_{mol}(\mu_1 r'')_1 dr'' \right\} dr'}{C * \beta_{mol}(\mu_1 r_{ref})_2} \\
& + \frac{\frac{RCS(\mu_2 r_{ref})}{C * \beta_{mol}(\mu_2 r_{ref})}_2 + 2 * S_a * \int_{\mu_2 r}^{\mu_2 r_{ref}} RCS(\mu_2 r')_2 * \exp \left\{ 2 * (S_a - S_m) * \int_{\mu_2 r}^{\mu_2 r_{ref}} \beta_{mol}(\mu_2 r'')_2 dr'' \right\} dr'}{C * \beta_{mol}(\mu_2 r_{ref})_2} \\
& = \frac{k * \exp(-2 \int_0^{\mu_1 r_{ref}} [\alpha_{aer}(\mu_1 r)_1 + \alpha_{mol}(\mu_1 r)_1] dr) + 2 * S_a * \int_{\mu_1 r}^{\mu_1 r_{ref}} k * (\beta_{aer}(\mu_1 r')_1 + \beta_{mol}(\mu_1 r')_1) * \exp(-2 \int_0^{\mu_1 r_{ref}} \alpha_{mol}(\mu_1 r'')_1 dr'') - 2 \int_0^{\mu_1 r} \alpha_{aer}(\mu_1 r'')_1 dr'') + 2 * S_a \int_{\mu_1 r}^{\mu_1 r_{ref}} \beta_{mol}(\mu_1 r'')_1 dr'')}{k * \exp(-2 \int_0^{\mu_2 r_{ref}} [\alpha_{aer}(\mu_2 r)_2 + \alpha_{mol}(\mu_2 r)_2] dr) + 2 * S_a * \int_{\mu_2 r}^{\mu_2 r_{ref}} k * (\beta_{aer}(\mu_2 r')_2 + \beta_{mol}(\mu_2 r')_2) * \exp(-2 \int_0^{\mu_2 r_{ref}} \alpha_{mol}(\mu_2 r'')_2 dr'') - 2 \int_0^{\mu_2 r} \alpha_{aer}(\mu_2 r'')_2 dr'') + 2 * S_a \int_{\mu_2 r}^{\mu_2 r_{ref}} \beta_{mol}(\mu_2 r'')_2 dr'')} \\
75 & = \frac{\exp(-2 \int_0^{\mu_1 r_{ref}} [\alpha_{aer}(\mu_1 r)_1 + \alpha_{mol}(\mu_1 r)_1] dr) + 2 * S_a * \int_{\mu_1 r}^{\mu_1 r_{ref}} [\beta_{aer}(\mu_1 r')_1 + \beta_{mol}(\mu_1 r')_1] * \exp(-2 \int_0^{\mu_1 r_{ref}} \alpha_{mol}(\mu_1 r'')_1 dr'') - 2 \int_0^{\mu_1 r} \alpha_{aer}(\mu_1 r'')_1 dr'') + 2 * S_a \int_{\mu_1 r}^{\mu_1 r_{ref}} \beta_{mol}(\mu_1 r'')_1 dr'')}{\exp(-2 \int_0^{\mu_2 r_{ref}} [\alpha_{aer}(\mu_2 r)_2 + \alpha_{mol}(\mu_2 r)_2] dr) + 2 * S_a * \int_{\mu_2 r}^{\mu_2 r_{ref}} [\beta_{aer}(\mu_2 r')_2 + \beta_{mol}(\mu_2 r')_2] * \exp(-2 \int_0^{\mu_2 r_{ref}} \alpha_{mol}(\mu_2 r'')_2 dr'') - 2 \int_0^{\mu_2 r} \alpha_{aer}(\mu_2 r'')_2 dr'') + 2 * S_a \int_{\mu_2 r}^{\mu_2 r_{ref}} \beta_{mol}(\mu_2 r'')_2 dr'')} \\
& = \frac{\exp(-2 \int_0^{\mu_1 r_{ref}} [\alpha_{aer}(\mu_1 r)_1 + \alpha_{mol}(\mu_1 r)_1] dr) + 2 * S_a * \int_{\mu_1 r}^{\mu_1 r_{ref}} [\beta_{aer}(\mu_1 r')_1 + \beta_{mol}(\mu_1 r')_1] * \exp\{-2 \int_0^{\mu_1 r_{ref}} [\alpha_{mol}(\mu_1 r'')_1 - S_a * \beta_{mol}(\mu_1 r'')_1] dr'') - 2 \int_0^{\mu_1 r} [\alpha_{aer}(\mu_1 r'')_1 + S_a * \beta_{mol}(\mu_1 r'')_1] dr'\}}{\exp(-2 \int_0^{\mu_2 r_{ref}} [\alpha_{aer}(\mu_2 r)_2 + \alpha_{mol}(\mu_2 r)_2] dr) + 2 * S_a * \int_{\mu_2 r}^{\mu_2 r_{ref}} [\beta_{aer}(\mu_2 r')_2 + \beta_{mol}(\mu_2 r')_2] * \exp\{-2 \int_0^{\mu_2 r_{ref}} [\alpha_{mol}(\mu_2 r'')_2 - S_a * \beta_{mol}(\mu_2 r'')_2] dr'') - 2 \int_0^{\mu_2 r} [\alpha_{aer}(\mu_2 r'')_2 + S_a * \beta_{mol}(\mu_2 r'')_2] dr'\}} \\
& = \frac{\exp(-2 \int_0^{\mu_1 r_{ref}} [\alpha_{aer}(\mu_1 r)_1 + \alpha_{mol}(\mu_1 r)_1] dr) + 2 * S_a * e^{-2 \int_0^{\mu_1 r_{ref}} [\alpha_{mol}(\mu_1 r'')_1 - S_a * \beta_{mol}(\mu_1 r'')_1] dr'') * \int_{\mu_1 r}^{\mu_1 r_{ref}} [\beta_{aer}(\mu_1 r')_1 + \beta_{mol}(\mu_1 r')_1] * e^{f(\mu_1 r)} dr}}{\exp(-2 \int_0^{\mu_2 r_{ref}} [\alpha_{aer}(\mu_2 r)_2 + \alpha_{mol}(\mu_2 r)_2] dr) + 2 * S_a * e^{-2 \int_0^{\mu_2 r_{ref}} [\alpha_{mol}(\mu_2 r'')_2 - S_a * \beta_{mol}(\mu_2 r'')_2] dr'') * \int_{\mu_2 r}^{\mu_2 r_{ref}} [\beta_{aer}(\mu_2 r')_2 + \beta_{mol}(\mu_2 r')_2] * e^{f(\mu_2 r)} dr} \quad (8)
\end{aligned}$$

As  $f'(r) = -2[S_{ain} * \beta_{aer}(r) + S_a * \beta_{mol}(r)]$  let  $S_{ain} = S_a$ , then  $f'(r) = -2 * S_a * [\beta_{aer}(r) + \beta_{mol}(r)]$

$$\int_r^{ref} B(r') * e^{f(r')} dr' = \int_r^{ref} \frac{f'(r')}{-2 * S_a} * e^{f(r')} dr' = \int_{f(r)}^{f(ref)} \frac{1}{-2 * S_a} * e^{f(r')} df(r') = \frac{1}{-2 * S_a} * e^{f(r')} \Big|_{f(r)}^{f(ref)} \quad (9)$$

$$80 \quad \int_{\mu_1 r}^{\mu_1 r_{ref}} B(\mu_1 r') * e^{f(\mu_1 r')} dr' = \frac{1}{-2 * S_a} * [e^{-2 * S_a * \int_0^{\mu_1 r_{ref}} [\beta_{aer}(\mu_1 r') + \beta_{mol}(\mu_1 r')] dr'} - e^{-2 * S_a * \int_0^{\mu_1 r} [\beta_{aer}(\mu_1 r') + \beta_{mol}(\mu_1 r')] dr'}] \quad (10)$$

$$\int_{\mu_2 r}^{\mu_2 r_{ref}} B(\mu_2 r') * e^{f(\mu_2 r')} dr' = \frac{1}{-2 * S_a} * [e^{-2 * S_a * \int_0^{\mu_2 r_{ref}} [\beta_{aer}(\mu_2 r') + \beta_{mol}(\mu_2 r')] dr'} - e^{-2 * S_a * \int_0^{\mu_2 r} [\beta_{aer}(\mu_2 r') + \beta_{mol}(\mu_2 r')] dr'}] \quad (11)$$

$$\begin{aligned}
& \frac{\exp(-2 \int_0^{\mu_1 r_{ref}} [\alpha_{aer}(\mu_1 r)_1 + \alpha_{mol}(\mu_1 r)_1] dr) + 2 * S_a * e^{-2 \int_0^{\mu_1 r_{ref}} [\alpha_{mol}(\mu_1 r'')_1 - S_a * \beta_{mol}(\mu_1 r'')_1] dr'') * \int_{\mu_1 r}^{\mu_1 r_{ref}} [\beta_{aer}(\mu_1 r')_1 + \beta_{mol}(\mu_1 r')_1] * e^{f(\mu_1 r)} dr}{\exp(-2 \int_0^{\mu_2 r_{ref}} [\alpha_{aer}(\mu_2 r)_2 + \alpha_{mol}(\mu_2 r)_2] dr) + 2 * S_a * e^{-2 \int_0^{\mu_2 r_{ref}} [\alpha_{mol}(\mu_2 r'')_2 - S_a * \beta_{mol}(\mu_2 r'')_2] dr'') * \int_{\mu_2 r}^{\mu_2 r_{ref}} [\beta_{aer}(\mu_2 r')_2 + \beta_{mol}(\mu_2 r')_2] * e^{f(\mu_2 r)} dr} \\
& = \frac{\exp(-2 \int_0^{\mu_1 r_{ref}} [\alpha_{aer}(\mu_1 r)_1 + \alpha_{mol}(\mu_1 r)_1] dr) - e^{-2 \int_0^{\mu_1 r_{ref}} [\alpha_{mol}(\mu_1 r'')_1 - S_a * \beta_{mol}(\mu_1 r'')_1] dr'') * e^{-2 * S_a * \int_0^{\mu_1 r} [\beta_{aer}(\mu_1 r') + \beta_{mol}(\mu_1 r')] dr'} - e^{-2 * S_a * \int_0^{\mu_1 r} [\beta_{aer}(\mu_1 r') + \beta_{mol}(\mu_1 r')] dr'}}{\exp(-2 \int_0^{\mu_2 r_{ref}} [\alpha_{aer}(\mu_2 r)_2 + \alpha_{mol}(\mu_2 r)_2] dr) - e^{-2 \int_0^{\mu_2 r_{ref}} [\alpha_{mol}(\mu_2 r'')_2 - S_a * \beta_{mol}(\mu_2 r'')_2] dr'') * e^{-2 * S_a * \int_0^{\mu_2 r} [\beta_{aer}(\mu_2 r') + \beta_{mol}(\mu_2 r')] dr'} - e^{-2 * S_a * \int_0^{\mu_2 r} [\beta_{aer}(\mu_2 r') + \beta_{mol}(\mu_2 r')] dr'}} \\
& = \frac{\exp(-2 \int_0^{\mu_1 r_{ref}} [\alpha_{aer}(\mu_1 r)_1 + \alpha_{mol}(\mu_1 r)_1] dr) - \exp(-2 \int_0^{\mu_1 r_{ref}} [\alpha_{aer}(\mu_1 r)_1 + \alpha_{mol}(\mu_1 r)_1] dr) + \exp\{-2 * S_a * \int_0^{\mu_1 r} [\beta_{aer}(\mu_1 r')_1 + \beta_{mol}(\mu_1 r')_1] dr' - 2 \int_0^{\mu_1 r_{ref}} [S_m * \beta_{mol}(\mu_1 r')_1 - S_a * \beta_{mol}(\mu_1 r')_1] dr'\}}{\exp(-2 \int_0^{\mu_2 r_{ref}} [\alpha_{aer}(\mu_2 r)_2 + \alpha_{mol}(\mu_2 r)_2] dr) - \exp(-2 \int_0^{\mu_2 r_{ref}} [\alpha_{aer}(\mu_2 r)_2 + \alpha_{mol}(\mu_2 r)_2] dr) + \exp\{-2 * S_a * \int_0^{\mu_2 r} [\beta_{aer}(\mu_2 r')_2 + \beta_{mol}(\mu_2 r')_2] dr' - 2 \int_0^{\mu_2 r_{ref}} [S_m * \beta_{mol}(\mu_2 r')_2 - S_a * \beta_{mol}(\mu_2 r')_2] dr'\}}
\end{aligned}$$

$$85 \quad = \frac{1}{\exp\{-2 \int_0^{\mu r_{ref}} [S_m * \beta_{mol}(r') - S_a * \beta_{mol}(r')] dr'\} \exp\{-2 * S_a * \int_0^{\mu r} [\beta_{aer}(r') + \beta_{mol}(r')] dr'\}} \quad (12)$$

If  $S_a = S_{ain}$ , the Ratio  $R = 1$ , which means that the backscatter coefficient profiles of two elevation angle are consistent. We can also see that  $S_a = S_{ain}$  is also the only solution for  $R = 1$ , which also means that we can indeed get the lidar ratio from this method.

**Table. S1 Extinction coefficients for different window types and different window lengths averaging over 4.0 km – 6.0 km**

(Mm <sup>-1</sup> )	82.5 m	157.5 m	307.5 m	457.5 m	607.5 m	1207.5 m
Rect. window	48 ± 32	49 ± 19	48 ± 11	49 ± 8	51 ± 5	53 ± 5
Hamming window	49 ± 36	48 ± 27	49 ± 14	49 ± 9	50 ± 6	51 ± 4
Hanning window	49 ± 37	48 ± 29	49 ± 16	49 ± 10	49 ± 7	51 ± 4
Kalman filter	46 ± 39	47 ± 14	46 ± 8	48 ± 8	48 ± 6	48 ± 5

90

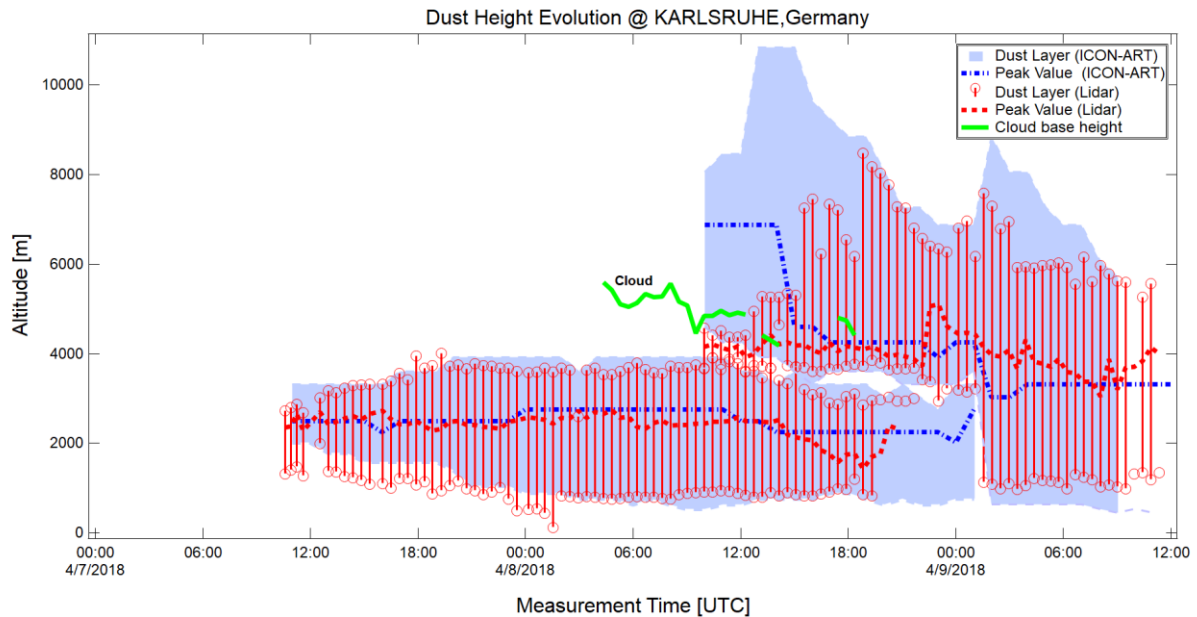


**Figure. S2 Time series of dust layer heights and peak heights (the heights for the maximum backscatter coefficients) for both lidar measurements and ICON-ART prediction as well as cloud base heights (green line) measured by lidar from 7<sup>th</sup> to 9<sup>th</sup>, April 2018.**

95

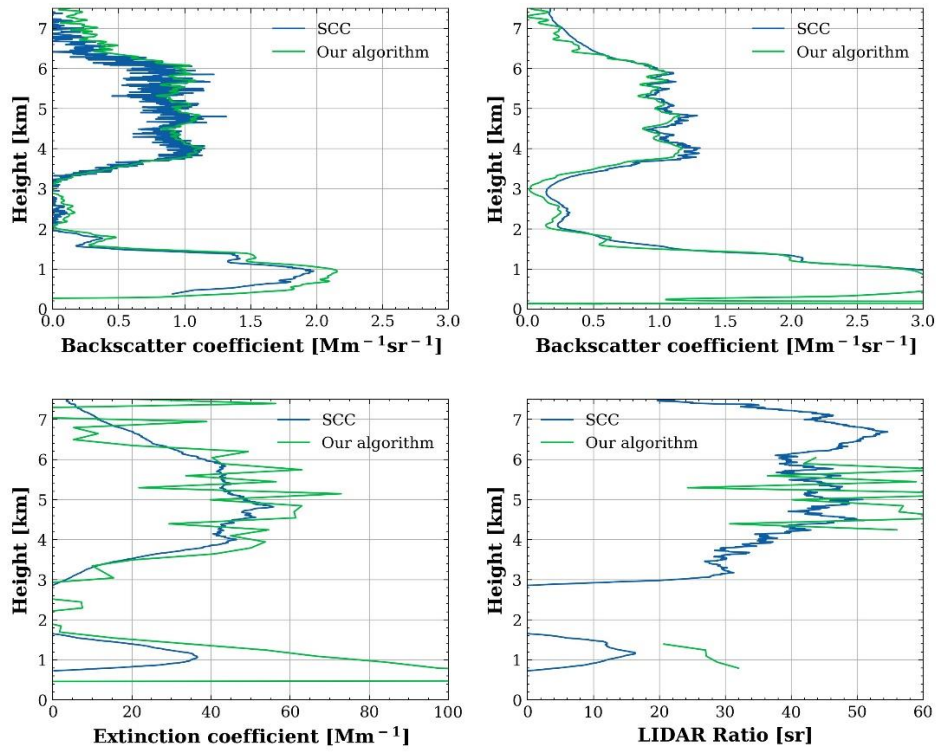
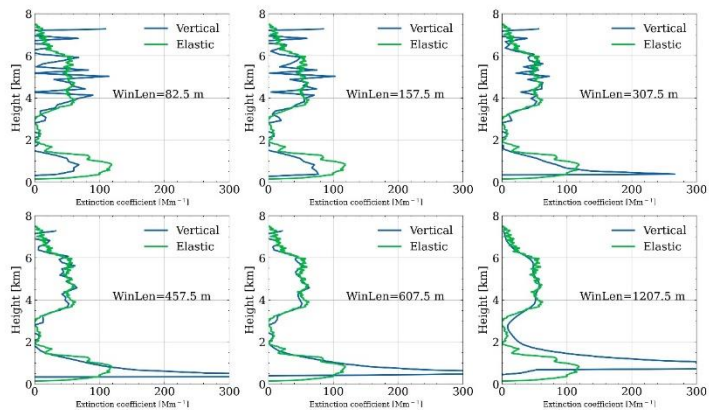
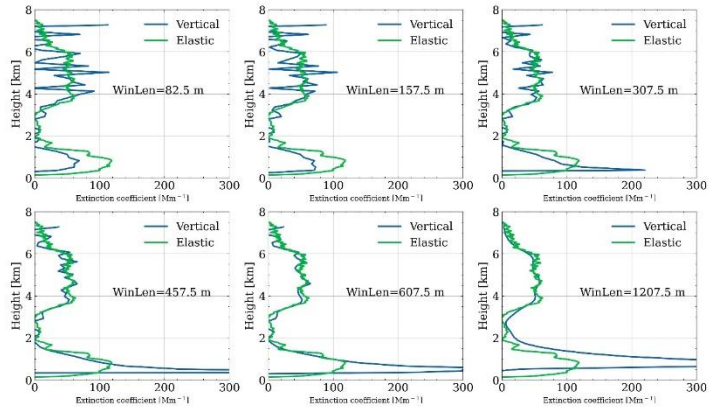


**Figure. S3** Elastic backscatter coefficient (a), Raman backscatter coefficient (b), Raman extinction coefficient (c) and lidar ratio (d) retrieved using the Single Calculus Chain (SCC) and our data algorithm (Kettle – Fernald).

2018-04-08 19:21:22:47 [UTC], Karlsruhe, Hamming window



2018-04-08 19:21:22:47 [UTC], Karlsruhe, Hanning window



100

2018-04-08 19:21:22:47 [UTC], Karlsruhe, Kalman Filter

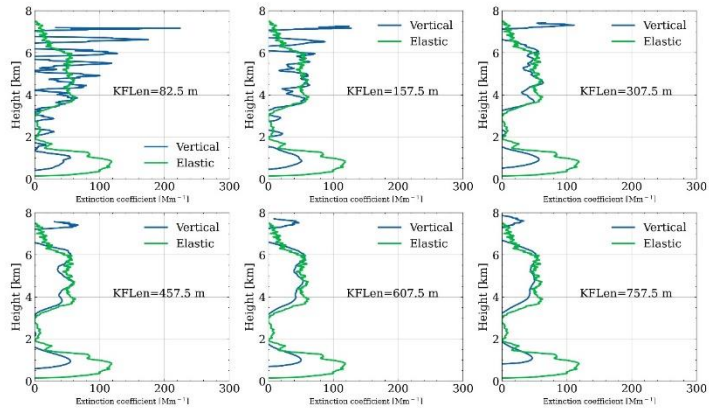


**Figure. S4 Vertical and slant extinction coefficients from Raman signal with different types of filters and different filter lengths**

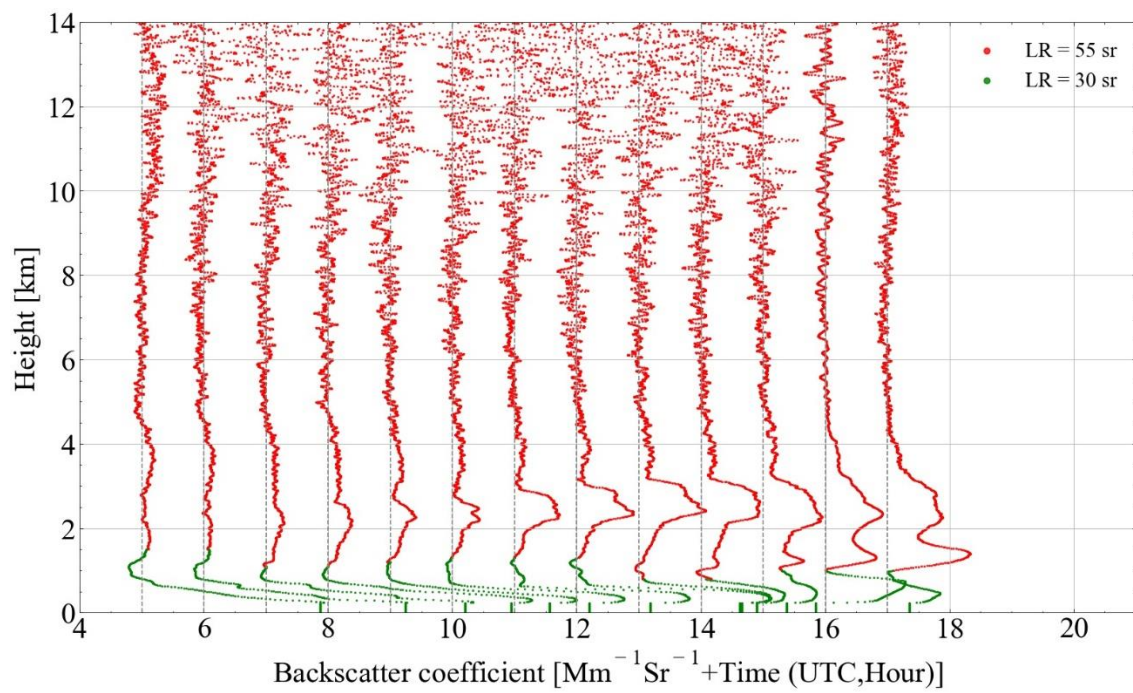


**Figure. S5 Elastic backscatter coefficients from vertical lidar measurement for different values of attitude-dependent lidar ratios  
with interval time being 1 hour**

105